

# A Teacher-Student MPC-PPO Coupled Reinforcement Learning Framework for Winter Temperature Control of Solar Greenhouses in Northern China

Jingxin Yu <sup>a,b,c</sup>, Lushun Ma <sup>c,d</sup>, Jinpeng Zhao <sup>c,d</sup>, Jianchao Ci <sup>b</sup>, Muhammad Abdul Munna<sup>b</sup>, Eldert van Henten<sup>b</sup>, Peter Groot Koerkamp<sup>b</sup>, Shuyi Peng<sup>b</sup>, Xiaoming Wei <sup>a,c,\*</sup>, Congcong Sun <sup>b,\*</sup>

<sup>a</sup> National Engineering Research Center for Intelligent Equipment in Agriculture, Beijing, 100097, China

<sup>b</sup> Agricultural Biosystems Engineering Group, Wageningen University, Wageningen, 6700 AA, The Netherlands

<sup>c</sup> Research Center for Intelligent Equipment Technology, Beijing Academy of Agriculture and Forestry Sciences, Beijing, 100097, China

<sup>d</sup> College of Mechanical and Electrical Engineering, Xi'an Technological University, Xi'an, 710021, China

\* Corresponding author.

E-mail address: [congcong.sun@wur.nl](mailto:congcong.sun@wur.nl) (C.Sun), [weixiaoming836@163.com](mailto:weixiaoming836@163.com) (X. Wei).

## Abstract

Solar greenhouses are crucial infrastructure of modern agricultural production in northern China. However, highly fluctuating temperature in winter season results in poor greenhouse temperature control, which affects crop growth and increases energy consumption. To tackle these challenges, an advanced control system that can efficiently optimize multiple objectives under dramatic climate conditions is essential. Therefore, this study propose a model predictive control-coupled proximal policy optimization (MPC-PPO) control framework. A teacher-student control framework is constructed in which the MPC generating high-quality control experiences to guide the PPO agent's learning process. An adaptive dynamic weighting mechanism is employed to balance the influence of MPC experiences during PPO training. Evaluation conducted in solar greenhouses across three provinces in northern China (Beijing, Hebei, and Shandong) demonstrates that: (1) the MPC-PPO method achieved the highest temperature control performance ( $96.31 \pm 4.71$  on a 100-point scale), with a 5.46-point improvement compared to the non-experience integration baseline, when reduced standard deviation by nearly half and enhanced exploration efficiency; (2) the MPC-PPO method achieved a ventilation control reward of  $99.19 \pm 0.54$ , optimizing ventilation window operations with intelligent time-differentiated strategies that reduced energy loss during non-optimal hours; (3) feature analysis reveals that historical window opening, air temperature, and historical temperature are the most influential features for effective control, i.e., SHAP values of 7.449, 4.905, and 4.747 respectively; and (4) cross-regional tests indicated that MPC-PPO performs best in all test regions, confirming generalization of the method.

# 1. Introduction

Chinese Solar Greenhouses (CSGs) are vital carriers of modern agricultural production in northern China. Statistics show that CSGs account for over 85% of the total greenhouse area nationwide and are primarily used to combat winter cold in northern regions, with concentrated distribution in major vegetable and fruit production areas such as Shandong, Hebei, and Liaoning (Fan et al., 2024). CSGs effectively utilize solar radiation to enable off-season crop cultivation during winter and spring, playing an important role in expanding the supply of agricultural products, particularly heat-sensitive vegetables, such as tomatoes, cucumbers, and leafy greens in winter, and promoting farmers' employment and income (Li et al., 2023). However, as production scales continue to expand, the cold winter climate in northern regions (with average outdoor temperatures often below  $-10^{\circ}\text{C}$ ) poses numerous challenges for greenhouse environmental control, including substantial heat loss through surfaces, extreme day-night temperature fluctuations (often exceeding  $20^{\circ}\text{C}$ ), and high energy consumption for maintaining minimal growing temperatures (He et al., 2025). Influenced by day-night temperature differences, the thermal environment inside greenhouses exhibits dramatic "cold-hot-cold" fluctuations (Bi et al., 2024). Without proper daytime temperature control, nighttime temperatures often fall excessively low, reducing plant recovery processes and slowing overall crop growth (Arshad et al., 2024). Both excessive and insufficient temperatures cause serious yield losses for heat-loving vegetables such as tomatoes and cucumbers (Shi et al., 2025). Meanwhile, greenhouse heating to maintain suitable temperatures can account for over 50% of total energy consumption (Abir Ahsan et al., 2025). Therefore, developing an advanced environmental control technology that efficiently meet objectives of optimized crop growth, balanced temperature and efficient energy use under dramatic climate conditions has become a critical scientific issue requiring attention.

In the field of multi-objective optimization, Model Predictive Control (MPC) has attracted attention for its powerful constraint handling and robust control capabilities (Mahmood et al., 2023). MPC combines historical data and future state of the controlled object, repeatedly iterating to solve for the optimal control sequence within a finite prediction horizon (Morato and Felix, 2024), unlike traditional Proportion-Integration-Differentiation (PID) controller that controls based only on the current state of the system. Due to rolling optimization mechanism, MPC can promptly respond to environmental disturbances and continuously suppress model mismatches, which is particularly valuable for complex greenhouse environmental control systems, gaining popularity in frequent applications. For instance, García-Mañas et al. (2024) developed a set of MPC-based models and controllers for Mediterranean coastal glass greenhouses, achieving precise tracking and control of greenhouse air temperature. Morcego et al. (2023) further incorporated Lettuce Greenhouse models, embedding crop growth dynamics into MPC prediction models, reducing temperature and humidity fluctuations in greenhouses to a great extent. Worth noting that MPC's performance largely depends on the accuracy of prediction models (Ding et al., 2018). In greenhouse applications, these prediction models typically incorporate heat and mass transfer functions, attempting to characterize complex thermodynamic relationships between internal air, structural components, and external environment (El Ghoumari et al., 2005). Due to cost and technical limitations, real-time data on greenhouse environments is often insufficient, making system identification and parameter estimation difficult, and thus prediction models struggle to accurately characterize the complex energy and material exchange processes inside greenhouses (Morcego et al., 2023). Additionally, MPC lacks active learning capabilities especially when environmental conditions and production needs a change dynamically. MPC cannot autonomously explore optimal control strategies, making it difficult to achieve multi-objective balance (Qi et al., 2024).

On the other side, Reinforcement Learning (RL) is known for sequential decision-making, offering a new perspective for solving complex control problems (Gautron et al., 2022). RL can learn optimal control strategies through continuously interacting with the environment in trial and error (Mallick et al., 2025). End-to-end learning paradigm allows RL avoiding the need for precise modeling of controlled objects and

demonstrating excellent environmental adaptability when dealing with nonlinear, time-varying systems (Goldenits et al., 2024). Most importantly, RL can balance multiple sub-objectives and seek optimal equilibrium under complex constraints (Platero-Horcajadas et al., 2024). In turn, RL has been widely applied in fields of autonomous controls such as robot control, self-driving, and smart grids (Ladosz et al., 2022). In greenhouse controls, Adesanya et al. (2024) employed deep-Q network algorithms to optimize PID model hyperparameters, achieving adaptive control of greenhouse temperature and humidity. Wang et al. (2020) developed a greenhouse climate control framework based on deep deterministic policy gradient, achieving coordination of multiple actuators (ventilation fans, heaters, carbon dioxide supplementation devices) by optimizing long-term returns. However, current RL also faces challenges in greenhouse environmental control. For instance, RL requires frequent interaction with the environment, requiring expensive and lengthy greenhouse experiments that struggle to support massive sample collection and policy iteration. Compared to RL algorithms like Asynchronous Advantage Actor-Critic (A3C), Proximal Policy Optimization (PPO) is robust in setting learning rates and discount factors with better training stability (Rio et al., 2024). Additionally, PPO employs importance sampling, avoiding drastic policy fluctuations and converging to optimal policies more quickly and smoothly in complex environments (Xu et al., 2024).

Therefore, to overcome MPC's limitations in model accuracy and RL's low sampling and exploration efficiency, we propose Teacher-Student MPC-PPO framework with three steps - experience enhancement - dynamic replacement - policy optimization - through deep integration of MPC and PPO policy optimization. Through progressive learning of high-quality experiences generated by MPC and using an adaptive method to transfer experience, we can balance multiple goals while aiming for the best results. This creates a combined ventilation control framework for greenhouse micro-climate, allowing MPC and PPO to complement each other and improve both decision accuracy and learning speed.

The research objectives include: (1) to analyze how different integration strategies affect training efficiency and temperature control performance of the MPC-PPO model; (2) to analyze the dynamic embedding mechanism of MPC experience and reveal how experience integration influences model performance; (3) to optimize input feature combination method and evaluate the contribution of each feature to control effectiveness; (4) to evaluate the model's generalization performance through cross-regional testing. Figure 1 illustrates the research background, challenges, objectives, and contributions of this work.

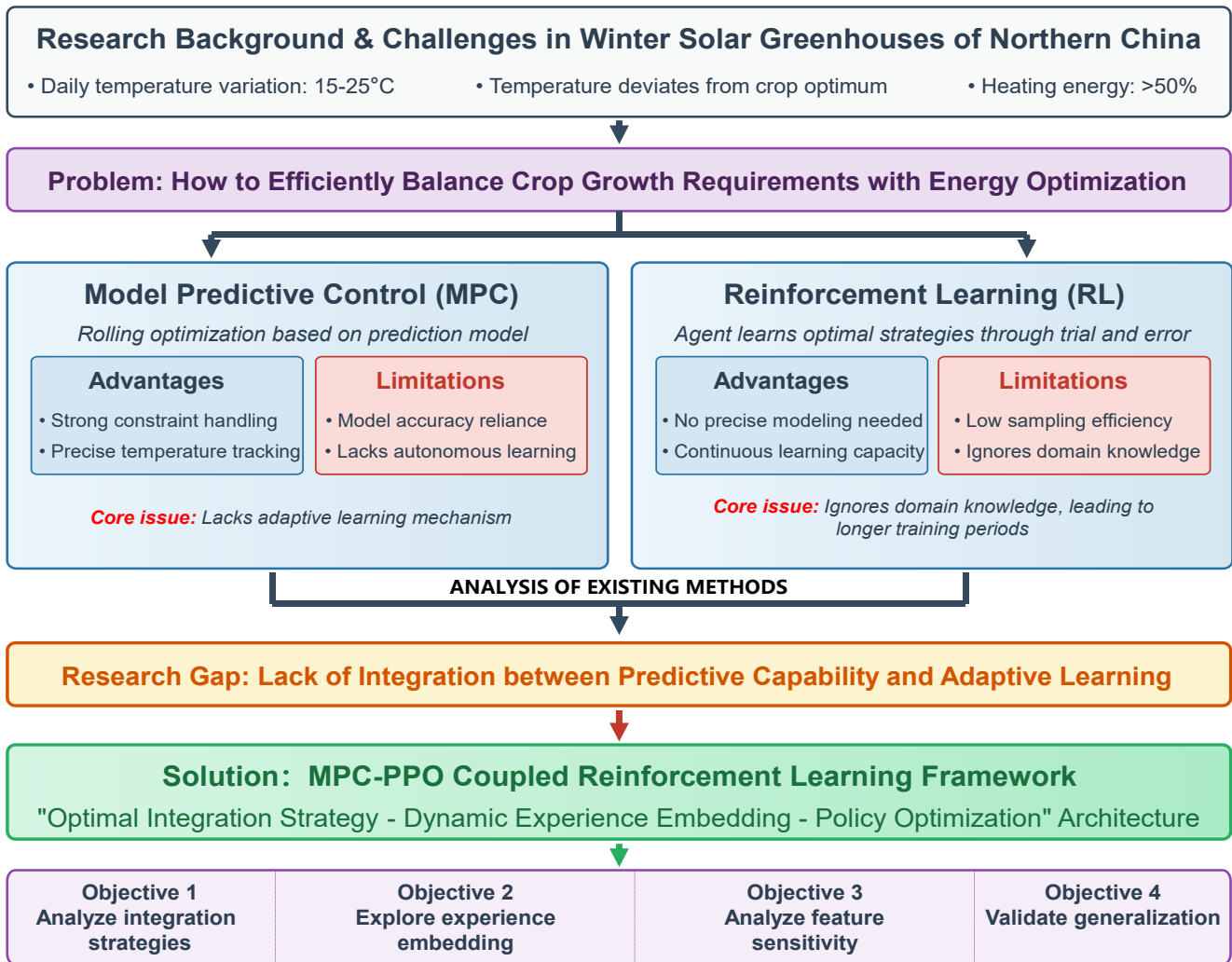
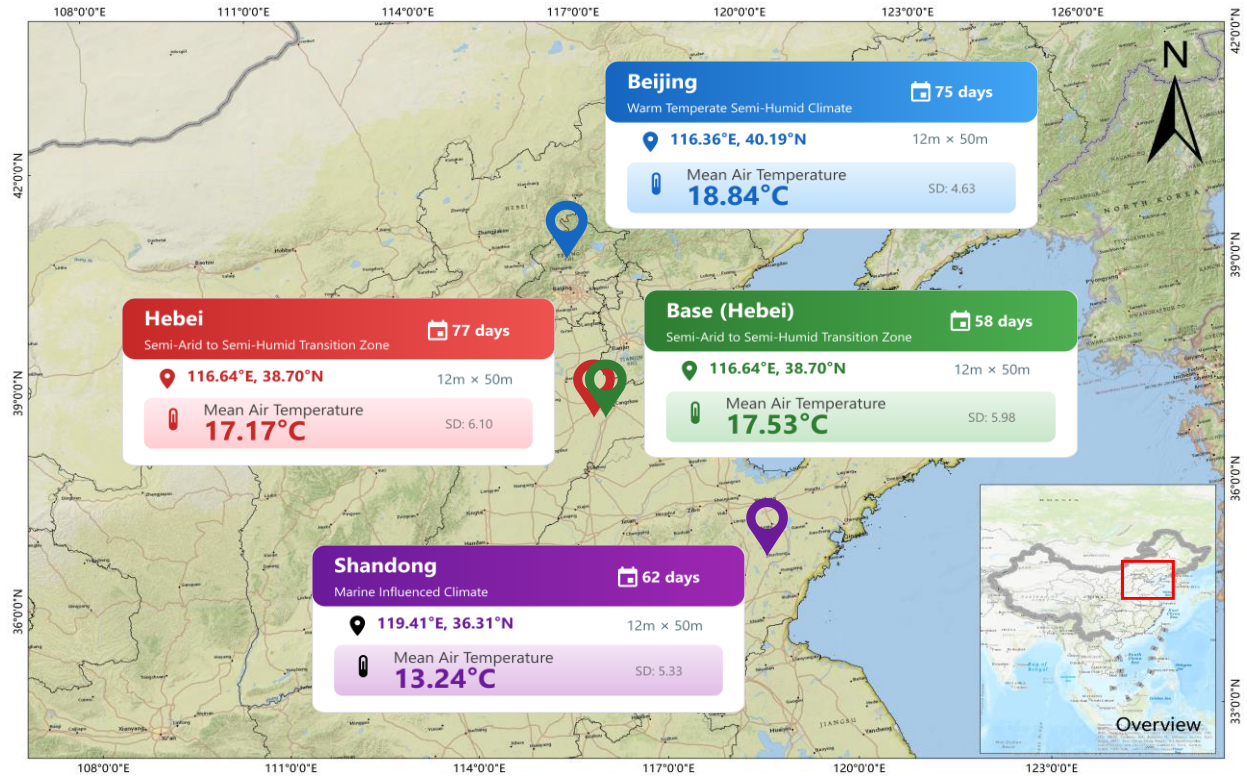


Fig. 1. Diagram of the MPC-PPO coupled reinforcement learning framework.

## 2. Materials

### 2.1 Study Area and Data Preparation

We selected four solar greenhouses across three provinces in northern China to evaluate the generalized performance of the MPC-PPO model (Figure 2). One greenhouse in Hebei Province (116.6371° E, 38.6994° N) provided benchmark data for training, while three greenhouses in Beijing (116.3597° E, 40.1851° N), Hebei (same complex), and Shandong (119.4050° E, 36.3051° N) served for generalization testing. These regions exhibit distinct climatic characteristics: Beijing has cold, dry winters with large day-night temperature variations; Hebei represents a semi-arid to semi-humid transition zone with lower winter temperatures; Shandong features higher humidity influenced by oceanic climate but experiences frequent cold waves.



**Fig. 2. Research area and greenhouse locations in China.**

All greenhouses feature east-west oriented prefabricated structures (12m span, 50m length) with soil cultivation and active heat storage systems including water walls. Sites were selected on flat terrain without surrounding obstructions to minimize external interference. During the study period, all greenhouses contained winter-stage crops and utilized PID control systems.

Environmental monitoring employed high-accuracy sensors including: air temperature sensors (Onset HOB0 MX2301A, LI-COR, Inc., Lincoln, NE, USA, accuracy  $\pm 0.2^{\circ}\text{C}$ ) positioned at 10-meter intervals along the longitudinal axis at 1.5m and 3.0m heights; water wall temperature sensors (Honeywell HSH-RM2ML, Honeywell International Inc., Charlotte, NC, USA, accuracy  $\pm 0.3^{\circ}\text{C}$ ) embedded in surfaces and circulation system nodes; soil temperature sensors (Onset S-TMB-M017,  $\pm 0.5^{\circ}\text{C}$  accuracy) buried at 10cm and 20cm depths and distributed at 5-meter intervals on both sides of furrows; and linear displacement sensors (KEYENCE GT2-H12, 0.5 $\mu\text{m}$  resolution) for ventilation opening measurement. All sensors connected to a central data collector (Onset RX3000) with 5-minute sampling frequency, continuously recording throughout the winter growing season.

## 2.2 Data Preprocessing

To ensure data quality and algorithm applicability, reasonable threshold intervals for sensor data were set based on expert experience (air temperature -5 to 50 $^{\circ}\text{C}$ , water tank temperature 0 to 80 $^{\circ}\text{C}$ , soil temperature 0 to 50 $^{\circ}\text{C}$ , wall temperature 0 to 40 $^{\circ}\text{C}$ , ventilation window opening 0 to 100%). Sliding median filtering (Kumar and Patel, 2023) (window width=5) was used to identify and process anomalies. For the very few missing data points in the original data (fewer than 5 entries), Kalman filtering (Wang et al., 2023) was applied for interpolation. For data standardization, min-max normalization (Kim et al., 2025) ( $X_{norm} = (X - X_{min}) / (X_{max} - X_{min})$ ) was used to process parameters of different dimensions. Using days as units (288 data points per day), a random strategy (seed set to 48 for all randomness throughout the paper) was employed to divide the dataset into training (80%) and testing (20%) sets, which has been shown to improve model generalization across varying environmental conditions in previous greenhouse modeling studies (Yu et al., 2025, 2020).

## 2.3 Explorative Data Analysis

The statistical analysis of thermal environment data from Beijing, Hebei, and Shandong greenhouses revealed distinct regional patterns (Table 1). The data was collected over specified periods (58-77 days in winter growing season from December 2023 to January 2024 for each site). Statistical measures included mean values, standard deviation (SD), minimum, median, maximum values, and coefficient of variation (CV). Air temperature in Hebei showed the highest SD (6.1°C), indicating more pronounced temperature fluctuations, while Shandong exhibited the greatest instability with the highest CV (40.28%). Water tank temperatures in both Hebei greenhouses showed significant variability (CV=62.15% and 61.49%), with maximum temperatures reaching 73.80°C, suggesting potential overheating risks. Soil temperatures were highest in Hebei greenhouses (means of 27.70°C and 29.53°C) with larger SDs (8.90°C and 8.16°C), indicating stronger external influences. Shandong soil temperatures showed moderate variability (CV=30.78%). Wall temperatures consistently exhibited lower CVs across all sites, demonstrating reduced sensitivity to environmental fluctuations due to building insulation properties. The high air temperature variability in Shandong (CV=40.28%) presented particular challenges for modeling and controlling the system.

**Table 1. Statistical analysis of greenhouse microclimate conditions in study period.**

Region	Parameter	Abbreviation	Unit	Mean	SD	Minimum	Median	Maximum	CV
Base (Hebei, 58 days)	Air Temperature	$T_{air}$	°C	17.53	5.98	6.50	15.10	46.90	34.12%
	Water Tank Temperature	$T_{water}$	°C	21.84	13.43	6.90	16.00	73.80	61.49%
	Soil Temperature	$T_{soil}$	°C	29.53	8.16	11.20	30.80	48.00	27.64%
	Wall Temperature	$T_{wall}$	°C	19.24	3.40	12.80	18.50	33.20	17.65%
	Window Opening	$\alpha_{vent}$	%	6.99	17.98	0.00	0.00	100.00	257.27%
Beijing (75 days)	Air Temperature	$T_{air}$	°C	18.84	4.63	8.50	18.40	40.30	24.59%
	Water Tank Temperature	$T_{water}$	°C	23.12	11.44	8.70	19.30	67.30	49.48%
	Soil Temperature	$T_{soil}$	°C	22.01	5.64	8.60	23.60	34.00	25.63%
	Wall Temperature	$T_{wall}$	°C	19.57	1.82	15.20	19.60	26.00	9.30%
	Window Opening	$\alpha_{vent}$	%	6.53	17.53	0.00	0.00	100.00	268.63%
Hebei (77 days)	Air Temperature	$T_{air}$	°C	17.17	6.10	5.20	15.00	46.90	35.54%
	Water Tank Temperature	$T_{water}$	°C	21.23	13.19	4.10	15.70	73.80	62.15%
	Soil Temperature	$T_{soil}$	°C	27.70	8.90	6.20	28.70	48.00	32.14%
	Wall Temperature	$T_{wall}$	°C	18.37	4.17	5.10	17.90	36.90	22.71%
	Window Opening	$\alpha_{vent}$	%	6.44	17.42	0.00	0.00	100.00	270.57%
Shandong (62 days)	Air Temperature	$T_{air}$	°C	13.24	5.33	4.50	12.10	33.70	40.28%
	Water Tank Temperature	$T_{water}$	°C	23.06	11.85	8.70	19.00	67.30	51.37%
	Soil Temperature	$T_{soil}$	°C	22.50	6.93	8.60	23.70	43.80	30.78%
	Wall Temperature	$T_{wall}$	°C	19.95	2.05	15.20	19.70	29.10	10.27%

Region	Parameter	Abbreviation	Unit	Mean	SD	Minimum	Median	Maximum	CV
	Window Opening	$\alpha_{vent}$	%	5.62	13.77	0.00	0.00	91.00	245.05%

## 3. Methods

### 3.1. Research Framework Overview

The MPC-PPO coupled control framework integrates complementary strengths of two control paradigms to address greenhouse temperature regulation challenges. MPC provides precise predictions and high-quality experiences based on system models, while RL enables adaptive learning through environmental interactions. The framework discretizes ventilation window openings into 11 levels (0%-100%, with 10% steps) to balance computational efficiency and control accuracy. As shown in Figure 3, the framework consists of four interconnected layers: 1) data processing layer, which collects greenhouse environmental data (temperature, ventilation) at 5-minute intervals and constructs a 10-dimensional state space; 2) MPC decision making layer, where the polynomial model enables real-time prediction and the MPC controller generates high-quality control experiences through rolling horizon optimization; 3) RL policy optimization layer, where a deep learning model provides a training environment, and the PPO policy network with an Actor-Critic architecture learns from the control experience generated by MPC while maintaining exploration capabilities to continuously improve its policy; 4) Performance evaluation layer, which employs a multi-objective reward function balancing temperature control (70%), ventilation efficiency (20%), action smoothness (5%), and temperature stability (5%).

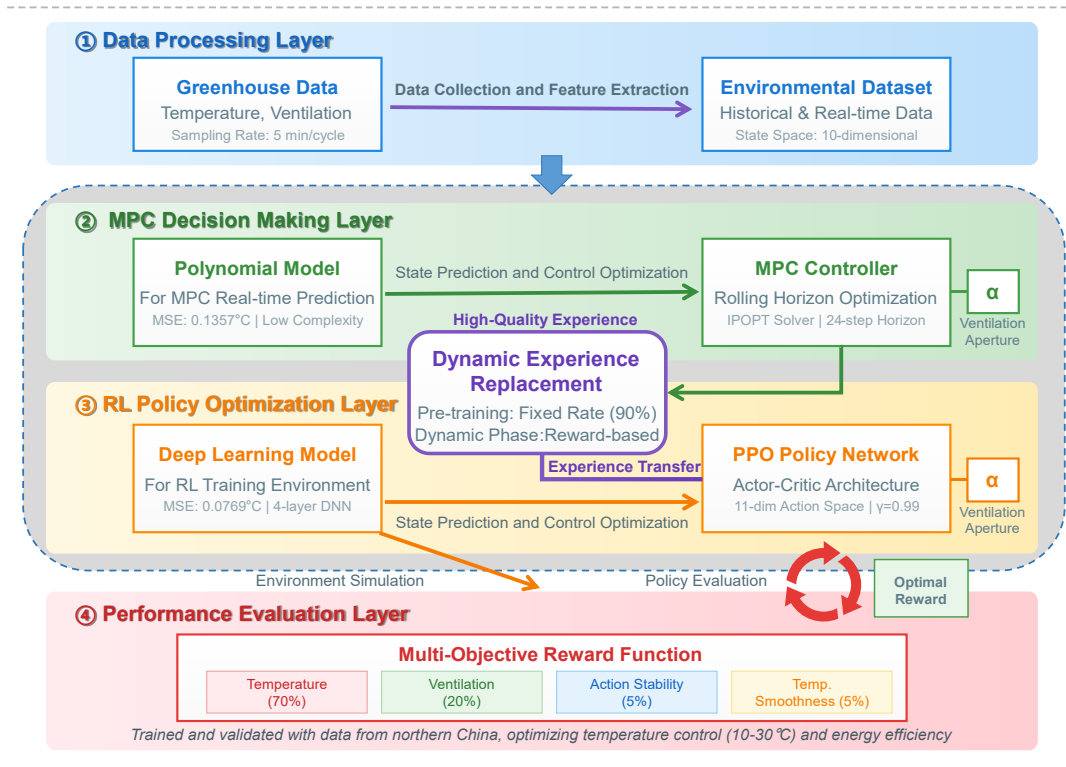


Fig. 3. Design of the MPC-PPO coupled reinforcement learning framework.

### 3.2 MPC Design

#### 3.2.1 Polynomial-based greenhouse environment model

The complex nonlinear characteristics of greenhouse environments can be captured to enable real-time prediction for the MPC controller. This study first develops a fast prediction model using second-order polynomial features. In this model, the dynamical features of greenhouse systems is characterized using state-space representation, the state vector  $X_t$  includes 10 key variables: air temperature  $T_{air}$ , soil temperature  $T_{soil}$ , water tank temperature  $T_{water}$ , wall temperature  $T_{wall}$ , ventilation window opening  $\alpha_{vent}$ , time features  $h, m, d$ , and historical statistical features  $\bar{T}$  (average air temperature inside the greenhouse from the beginning of the day to the decision-making time point) and  $\bar{\alpha}$  (average ventilation window opening from the beginning of the day to the decision-making time point). The value range of the state space is strictly limited within physical constraints:

$$X_t \in [0, 50]^4 \times [0, 100] \times [0, 23] \times [1, 12] \times [1, 31] \times [0, 50] \times [0, 100] \quad (1)$$

The state transition function adopts a polynomial feature expansion form, capturing nonlinear relationships between variables through cross-terms:

$$X_{t+1} = f(X_t, u_t) = \sum_{i=1}^n \sum_{j=1}^n \theta_{ij} x_{i,t} x_{j,t} + \sum_{k=1}^n \beta_k x_{k,t} + \gamma \quad (2)$$

where  $X_{t+1}$  represents the predicted state vector at the next time step,  $X_t$  is the current state vector,  $u_t$  is the control input (ventilation window opening percentage),  $x_{i,t}$  and  $x_{j,t}$  are elements of the state vector at time  $t$ ,  $n$  is the number of state variables,  $\theta_{ij}$  and  $\beta_k$  are model parameters obtained through least squares regression on historical data, and  $\gamma$  is a constant bias term.

### 3.2.2 MPC controller

The MPC controller performs prediction and optimization based on the polynomial environment model, adopting a 24-step rolling horizon optimization strategy, with the control objective function as shown in Equation 3.

$$\min_{u_t} \sum_{k=0}^{23} \left[ w_1 (T_k - T_{ref})^2 + w_2 (\Delta u_k)^2 + w_3 \phi(h_k) u_k \right] \quad (3)$$

where  $T_{ref} = 22^\circ C$  is the target temperature,  $\phi(h_k)$  is a time-related ventilation penalty function, and constraint conditions are the same as previously defined.

To ensure real-time performance, the model employs the IPOPT solver for optimization (Kyriakidis et al., 2024), setting the maximum iteration count to 100 and the convergence threshold to  $1e^{-4}$ . These settings satisfy real-time control requirements while ensuring prediction accuracy.

## 3.3 RL Design

### 3.2.2 Deep learning-based environment simulation model

To develop a high-fidelity greenhouse environment model with improved prediction accuracy for RL training, we designed a deep learning-based model, leveraging its superior ability to capture nonlinear dynamics and complex temporal dependencies in greenhouse environments. The four-layer neural network architecture (with 256, 128, and 64 neurons in hidden layers) was selected based on empirical testing, providing an optimal balance between model complexity and prediction accuracy for greenhouse thermal dynamics. Each hidden layer uses ReLU activation, with first layer employing batch normalization and 0.1 dropout. The forward propagation through each layer  $l$  follows:

$$z^{(l)} = W^{(l)} a^{(l-1)} + b^{(l)} \quad (4)$$

$$a^{(l)} = g^{(l)}(z^{(l)}) \quad (5)$$

where  $W^{(l)}$  is weights matrix,  $b^{(l)}$  is bias vector,  $g^{(l)}$  is activation function,  $a^{(l)}$  is layer activation, and  $a^{(0)}$  represents input features.

Training utilized Adam optimizer, Mean Squared Error (MSE) loss function, and validation-based early stopping, with 8:2 training-validation split ratio.

### 3.2.3 Multi-objective reward function design

To achieve optimal control of greenhouse environments, a comprehensive multi-objective reward function was designed, balancing temperature control accuracy, system stability, and energy efficiency through weighted combinations. This study designs a multi-objective reward function that effectively balances temperature control accuracy, ventilation efficiency, action smoothness, and temperature stability. Through appropriate weight allocation based on agronomic requirements and control theory analysis, the reward function guides the reinforcement learning algorithm toward optimal greenhouse control. The design framework of the multi-objective reward function establishes a complete decision optimization system, integrating theoretical foundations with implementations, with specific weight allocations detailed in Equation 6.

$$R_{total} = 0.7R_{temp} + 0.2R_{vent} + 0.05R_{action} + 0.05R_{change} \quad (6)$$

where  $R_{temp}$ ,  $R_{vent}$ ,  $R_{action}$ , and  $R_{change}$  represent rewards for temperature control, ventilation control, action smoothness, and temperature change smoothness, respectively, calculated as shown in Equations 6-9. The detailed justification for the weight allocation is elaborated in Table 2.

Temperature control reward (Equation 7) reflects the accuracy of greenhouse temperature control, with higher rewards indicating longer periods of maintaining temperature within the target range.

$$R_{temp} = 100 \times \left(1 - \frac{N_{violations}}{N_{total}}\right) \quad (7)$$

where  $N_{violations}$  represents the number of time steps when temperature exceeds the allowed range [10°C, 30°C], and  $N_{total}$  is the total number of time steps (288steps·day<sup>-1</sup>).

Ventilation control reward (Equation 8) adopts a time-differentiated penalty mechanism. The smaller penalty (0.5) during optimal ventilation hours [8,17] encourages necessary daytime ventilation for temperature regulation, while the larger penalty (2.0) during non-optimal hours discourages unnecessary night ventilation that could lead to excessive heat loss in winter conditions.

$$R_{vent} = \begin{cases} 100 - 0.5|\alpha|, & \text{if } h \in [8,17] \\ 100 - 2.0|\alpha|, & \text{otherwise} \end{cases} \quad (8)$$

where  $\alpha$  is the ventilation window opening (%), and  $h$  is the current hour in 24-hour format.

Action smoothness reward (Equation 9) protects actuators by limiting frequent adjustments while ensuring control policy smoothness.

$$R_{action} = 100 \times \left(1 - \min\left(\frac{N_{changes}}{N_{max}}, 1\right)\right) \quad (9)$$

where  $N_{changes}$  is the number of ventilation window adjustments within a day, and  $N_{max}$  is set to 48 times/day (average once every 30 minutes).

Temperature stability reward (Equation 10) is used to avoid dramatic temperature fluctuations, ensuring stability of the crop growth environment. Each day has 288 time steps (5 minutes/step), and stability is maintained by limiting temperature changes between adjacent time steps.

$$R_{change} = 100 \times \left(1 - \frac{N_{excessive}}{N_{total}}\right) \quad (10)$$

where  $N_{excessive}$  is the number of time steps when the temperature change rate exceeds 5°C/5 minutes.

The specific parameter settings in Table 2, including temperature constraint ranges, ventilation time periods, and penalty coefficients, were determined based on extensive practical experience in managing solar greenhouses in northern China and iterative field testing during different growing seasons. The weights of the reward function (temperature control: 0.7, ventilation control: 0.2, action smoothness: 0.05, temperature stability: 0.05) were established through agronomic experiments and control theory analysis. This allocation reflects greenhouse control priorities: temperature control receives highest weight as the critical crop growth factor, ventilation control ranks second as a key energy management mechanism, while smoothness indicators receive moderate weights to ensure system stability and reliability. This structure demonstrated an optimal multi-objective balance in experiments, enabling the RL algorithm to improve energy efficiency and system stability while maintaining temperature control accuracy.

**Table 2. Multi-objective reward function parameter settings.**

Parameter Type	Constraint Range	Weight Coefficient	Scoring Rule
Temperature Control	[10, 30]°C	0.7	Temperature exceeding target range counted as violation, lower violation ratio yields higher reward, reward range [0,100]
Ventilation Control	[0, 100]%	0.2	Base reward 100, during [8,17] period each 1% opening deducts 0.5 points, other periods each 1% opening deducts 2.0 points
Action Smoothness	≤48 times/day	0.05	Ventilation window adjustment frequency not exceeding 48 times/day, exceeding reduces reward proportionally, reward range [0,100]
Temperature Stability	≤5°C/5min	0.05	Adjacent time step (5 minutes) temperature change not exceeding 5°C, exceeding counted as dramatic fluctuation, lower fluctuation ratio yields higher reward, reward range [0,100]

### 3.3.2 PPO policy network

The policy network employs a deep neural network structure (Figure 5), with both Actor and Critic networks using the 7-layer feed-forward network architecture [512-256-256-128-64-32-16]. The 7-layer architecture was selected after extensive comparative testing, providing sufficient representation capacity for the complex greenhouse control problem while maintaining computational efficiency. Each layer uses ReLU (Xu and Zhang, 2024) activation function and adopts the AdamW (Zhou et al., 2024) optimizer to improve training stability. The Actor network ultimately outputs an 11-dimensional action probability distribution (Softmax activation), corresponding to 11 discrete ventilation window opening options from 0% to 100%; the Critic network outputs state value estimates (linear activation).

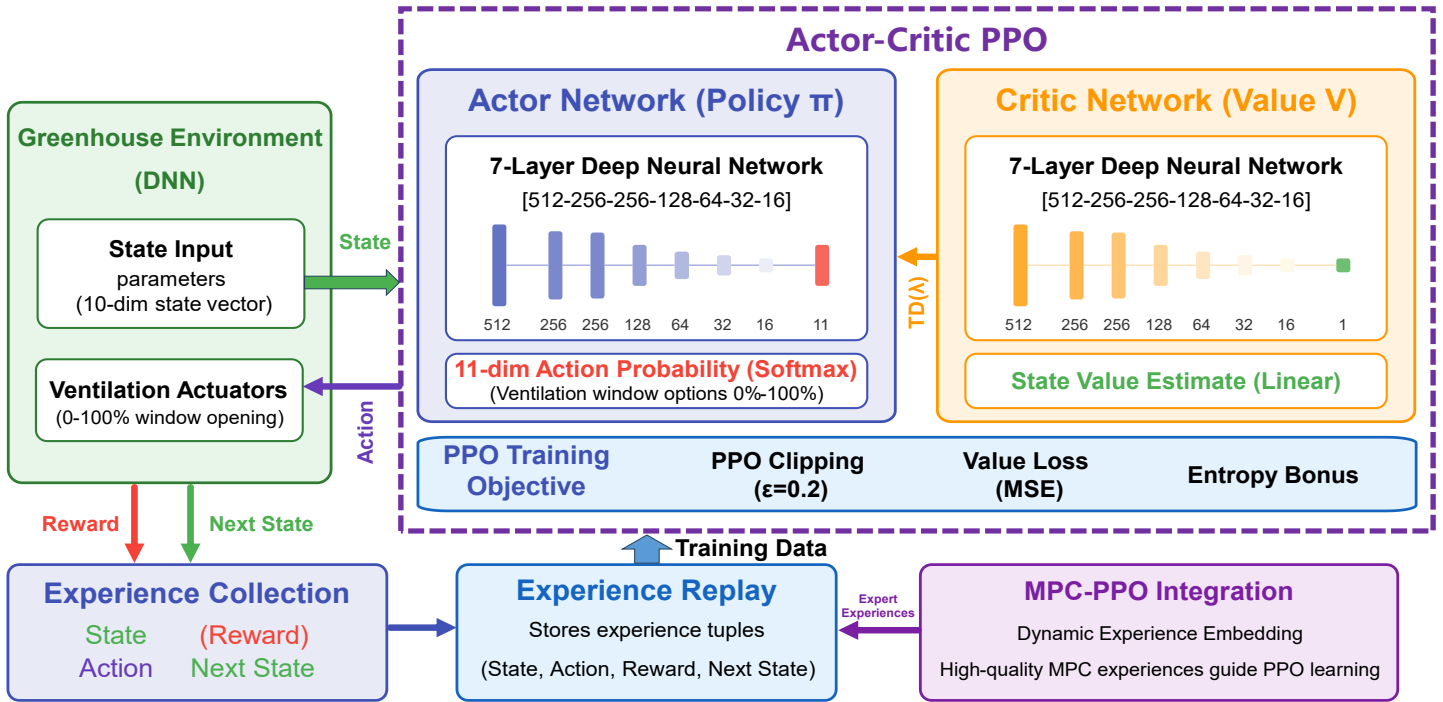


Fig. 5. Actor-critic network architecture in PPO policy network

Policy updates adopt the PPO clipping objective, ensuring training stability by limiting policy update step sizes, as shown in Equation 11.

$$L^{CLIP}(\theta) = \hat{\mathbb{E}}_t [\min(r_t(\theta)\hat{A}_t, clip(r_t(\theta), 1 - \epsilon, 1 + \epsilon)\hat{A}_t)] \quad (11)$$

where  $\epsilon = 0.2$  is the clipping parameter, preventing drastic policy changes while ensuring exploration (Zhu and Rosendo, 2021).

The hyperparameter settings for the PPO algorithm are shown in Table 3. These parameters have been thoroughly validated through experiments and can achieve stable, efficient policy learning in complex environments.

Table 3. Hyperparameter settings in PPO algorithm.

Parameter Name	Value	Description
Number of Parallel Environments	20	Improves sampling efficiency and training stability
Batch Size	28800	Number of samples per policy update
Training Epochs	4000	Number of iterations for complete training process
Learning Rate	$3e^{-4}$	Step size for policy network parameter updates
PPO Clipping Parameter	0.2	Limits policy update magnitude
Discount Factor	0.99	Decay coefficient for future rewards
GAE Parameter	0.95	Smoothing coefficient for advantage estimation
Sampling Steps	2880	Sampling length for each environment
Network Update Rounds	4000	Training iterations per batch of data

## 3.4 MPC-PPO Coupled Framework

### 3.4.1 Teacher-student integration mechanism

To further improve exploration efficiency of RL algorithm, an integrated teacher-student MPC-PPO framework was designed (Figure 6), divided into “experience enhancement - dynamic replacement - policy optimization” three steps: 1) Generation of high-quality experiences from MPC into an experience pool, considered as expert teacher data; 2) A phased replacement strategy with pre-training and dynamic replacement phases, optimizing the training process through different replacement mechanisms; 3) PPO policy learning guided by these experiences through adaptive experience transfer, which dynamically determines when and how to incorporate MPC knowledge. This teacher-student framework enables effective knowledge transfer from model-based optimization to data-driven learning while maintaining necessary exploration capabilities. During the pre-training phase (first 2 training rounds), a high proportion (90%) experience replacement strategy was adopted, rapidly establishing a foundation policy through massive injection of high-quality historical experiences. The replacement during the pre-training phase did not consider current policy performance but maintained a fixed replacement ratio to accelerate initial policy convergence. In the dynamic replacement phase (starting from the 3rd training round), the system transitions to a reward-based selective replacement strategy. The replacement probability  $p(replace|s_t, a_t, r_t)$  was calculated based on the episode’s total reward  $R_{episode}$ , as shown in Equation 12.

$$p(replace|s_t, a_t, r_t) = \begin{cases} 1, & \text{if } R_{episode} < R_{threshold} \\ 0, & \text{otherwise} \end{cases} \quad (12)$$

To ensure the effectiveness of experience transfer, importance weights  $w(s_t, a_t)$  were used for correction, as shown in Equation 13. Through clipping of importance sampling weights, the influence of experience replacement on policy updates was restricted to a reasonable range.

$$w(s_t a_t) = \min \left( \max \left( \frac{\pi_{\theta}(a_t|s_t)}{\pi_{\beta}(a_t|s_t)}, 0.99 \right), 1.01 \right) \quad (13)$$

The default experience replacement mechanism’s core parameters included maximum experience pool capacity of 10000 episodes, replacement threshold of 90.0 points, and weight clipping range [0.99,1.01]. The system dynamically monitored poorly performing episodes (rewards below threshold) in each training round and selectively replaced only these episodes. The adaptive experience replacement mechanism was designed to accelerate policy learning progress while avoiding potential policy degradation issues from excessive replacement.

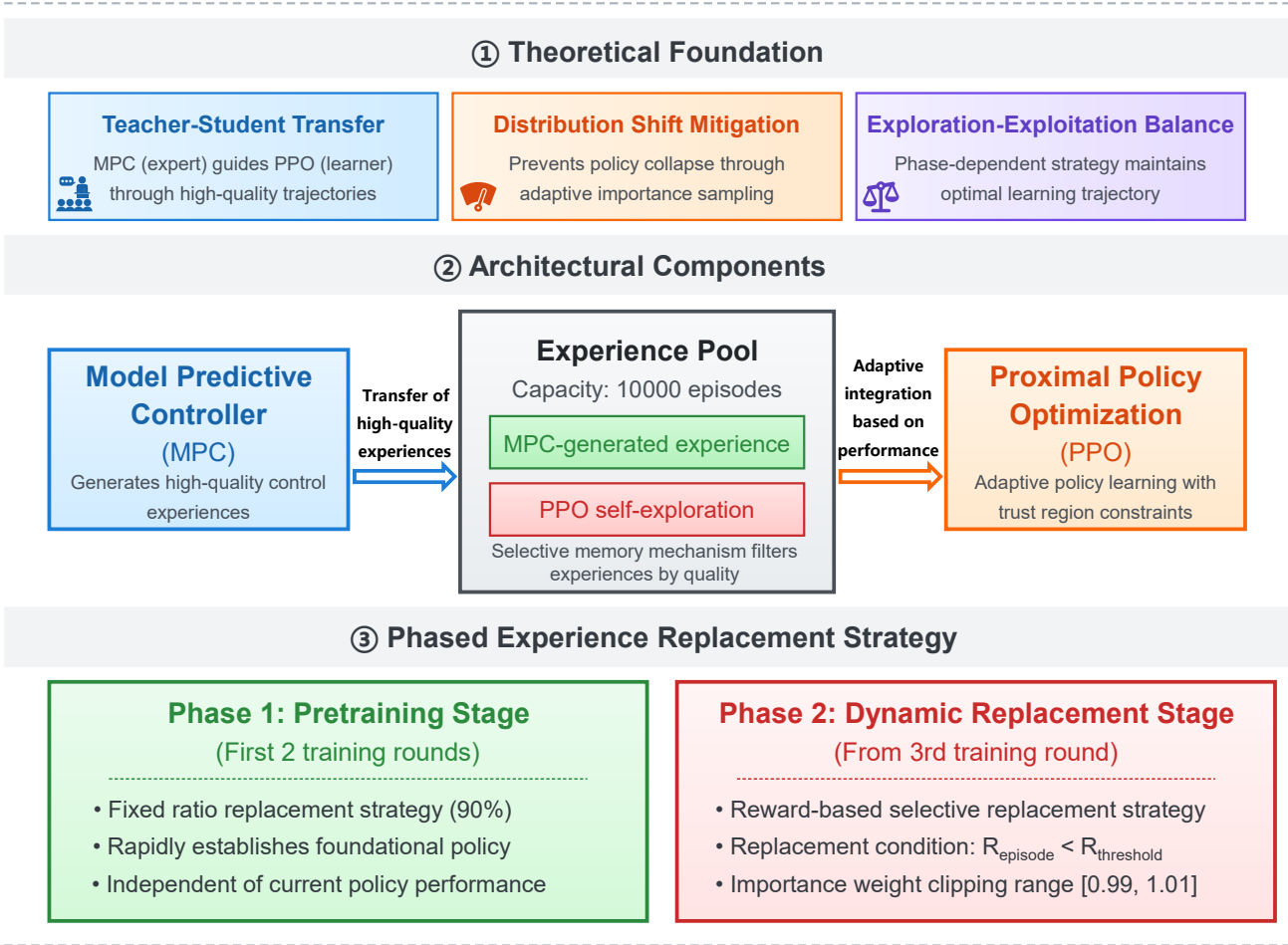


**Fig. 6. Experience dynamic replacement mechanism of the MPC-PPO coupled framework.**

### 3.4.2 Feature importance analysis

To analyze the influence of environmental parameters on control performance, we employed feature importance analysis based on SHAP values (Wang et al., 2025). This approach, implemented through gradient boosting models, quantifies each input feature's contribution to model output by measuring how each feature changes the expected prediction when included in different feature subsets. The method is particularly suitable for greenhouse control analysis as it can handle nonlinear relationships among parameters and control performance while providing interpretable importance rankings. The SHAP value for feature  $i$  is calculated as:

$$\phi_i(f, \mathbf{x}) = \sum_{S \subseteq N \setminus \{i\}} \frac{|S|!(|N|-|S|-1)!}{|N|!} [f_{\mathbf{x}}(S \cup \{i\}) - f_{\mathbf{x}}(S)] \quad (14)$$

where  $\phi_i$  represents feature  $i$ 's SHAP value,  $N$  is all features' set,  $S$  is a feature subset excluding feature  $i$ , and  $f_{\mathbf{x}}(S)$  is the prediction using only features in set  $S$ .

## 3.5. Experimental Environment Configuration

Experiments utilized a unified software and hardware environment for implementation efficiency and reproducibility. The software stack included Python 3.8, PyTorch 2.0 (deep learning), Gymnasium 0.28 and Stable-baselines3 (RL), CasADi 3.5.5 (MPC optimization), NumPy 1.21 and Pandas 1.5 (data processing), and TensorBoard 2.10 (visualization). The training process employed carefully tuned parameters: 40 million total training steps, 20 parallel environments for sampling (2880 steps each, equivalent to one day), and batch size of 28800. Performance assessment occurred every 57600 steps (20 days), with each assessment repeated five times. An early stopping mechanism terminated training after 200 consecutive

rounds without improvement. The system saved both the final model and the highest-scoring version. Hardware configuration included an Intel Core i9 processor, NVIDIA RTX 4090 GPU, 64GB RAM, and Windows Server 2016. CUDA acceleration enhanced training performance, with TensorBoard monitoring key metrics including loss trends, evaluation rewards, experience replacement ratios, and resource utilization.

## 4. Results and Discussion

### 4.1 Environment Model Performance

The prediction accuracy of polynomial model and deep learning model is shown in Figure 7. Polynomial model achieved a MSE of  $0.1357^{\circ}\text{C}$ , satisfying the MPC controller's balance requirements between computational speed and prediction accuracy. Besides, deep learning model observed an MSE of  $0.0769^{\circ}\text{C}$ , improving prediction accuracy by about 43.3% compared to the polynomial model and thus providing reliable environmental simulation for RL training.

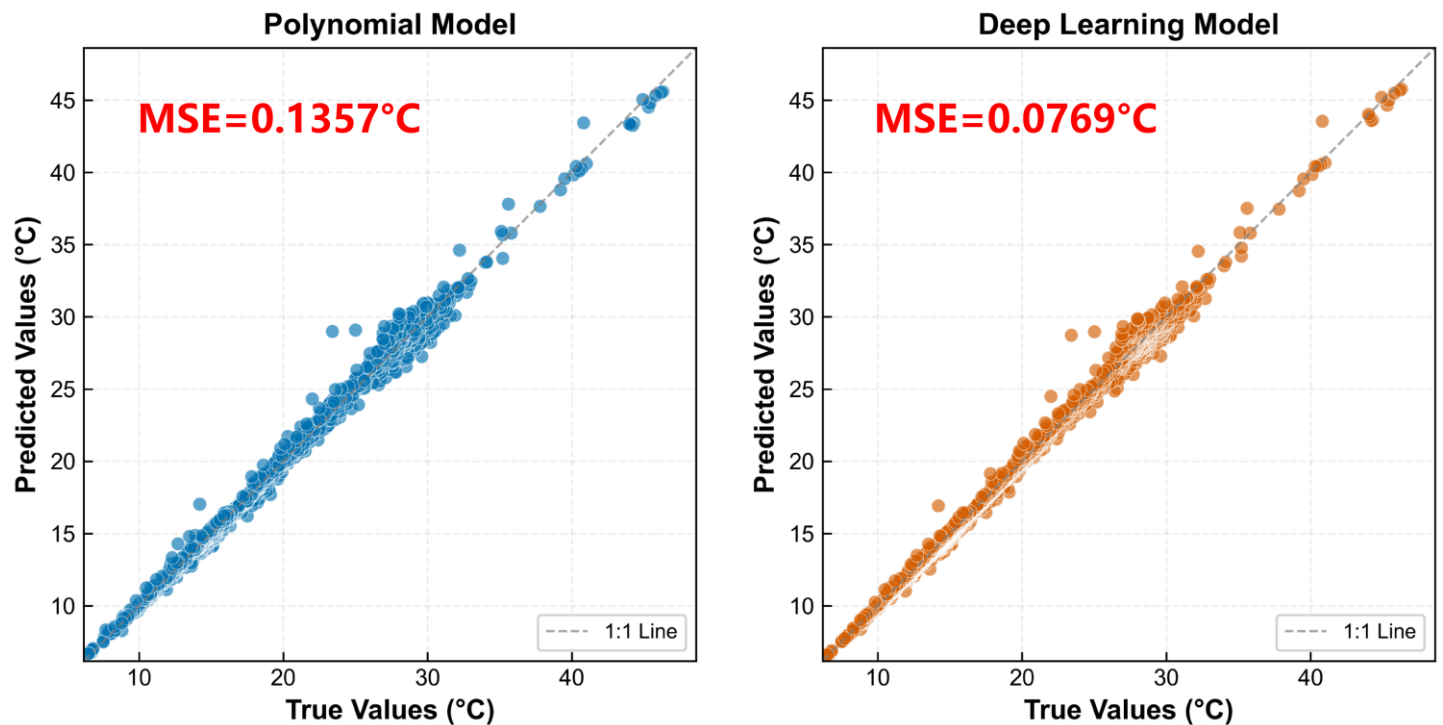


Fig. 7. Performance comparison between polynomial model and deep learning model.

### 4.2 MPC-PPO Control Performance

#### 4.2.1 Temperature control

Table 4 shows the performances of the MPC-PPO coupled controls in greenhouse environment. Rewards for the various control methods varied between 79.34 and 100.00, with the proposed MPC-PPO demonstrating significant advantages in overall performance. The MPC-PPO method outperformed other methods with final rewards of  $96.31 \pm 4.71$ , achieving both the highest control accuracy and stability.

For the temperature control reward (70% weight), the MPC-PPO method achieved the highest reward of 94.99 with the smallest fluctuation range ( $\pm 6.66$ ), improving by 2.8 points and nearly halving the standard deviation compared to traditional MPC method ( $92.19 \pm 12.80$ ). The PPO method with lower reward (89.53) than MPC showed high stability ( $\pm 9.86$ ), demonstrating the potential of RL in ensuring

stable environment. The traditional PID controller showed the lowest accuracy and greatest fluctuation ( $88.34 \pm 16.14$ ).

#### 4.2.2 Action smoothness and temperature stability

MPC, PPO, and MPC-PPO achieved high rewards of 99.65 with minimal fluctuation ( $\pm 0.81$ ) in action smoothness, indicating their effectiveness in avoiding frequent adjustments and extending actuator lifespan. In contrast, reward of PID controller was significantly low ( $79.34 \pm 29.13$ ) and highly fluctuating, which reflects instability of traditional control methods at complex environments. Besides, both MPC-PPO and PID methods achieved perfect rewards of 100.00 with no fluctuation ( $\pm 0.00$ ) for temperature changes and capable to deal with dramatic temperature fluctuations.

#### 4.2.3 Ventilation control

MPC achieved the highest reward ( $99.36 \pm 0.49$ ) for ventilation control followed by MPC-PPO ( $99.19 \pm 0.54$ ). The minor difference explains the ability of MPC achieving near-optimal control effects within short time windows. However, MPC-PPO sacrifices slightly in single-point accuracy but gains strong environmental adaptability through the generalization capability of policy networks.

**Table 4. Performance comparison of different control strategies.**

Method	temp_reward (70%)	action_reward (5%)	change_reward (5%)	ventilation_reward (20%)	Final reward
PID	$88.34 \pm 16.14$	$79.34 \pm 29.13$	$100.00 \pm 0.00$	$97.08 \pm 3.88$	$90.22 \pm 11.85$
MPC	$92.19 \pm 12.80$	$99.65 \pm 0.81$	$99.91 \pm 0.16$	$99.36 \pm 0.49$	$94.38 \pm 8.94$
PPO	$89.53 \pm 9.86$	$99.65 \pm 0.81$	$99.88 \pm 0.17$	$99.02 \pm 0.51$	$92.45 \pm 6.95$
MPC-PPO	$94.99 \pm 6.66$	$99.65 \pm 0.81$	$100.00 \pm 0.00$	$99.19 \pm 0.54$	$96.31 \pm 4.71$

#### 4.2.4 Learning efficiency

Figure 8 shows smoothed curves of test rewards during the training process for MPC-PPO and PPO algorithms. The proposed MPC-PPO model reaches a stable state in less than 10M training steps with relatively smoother overall process fluctuations. Meanwhile, the standard PPO model shows wave-like improvement, reaching stability around 35M steps, requiring about 3.5 times the computational resources of the MPC-PPO model.

MPC-PPO achieved efficient decision balancing by integrating forward-looking plan with long-term reward maximization, highly consistent with views reported by Mallick et al. (2025) about complementarity between predictive control and RL.

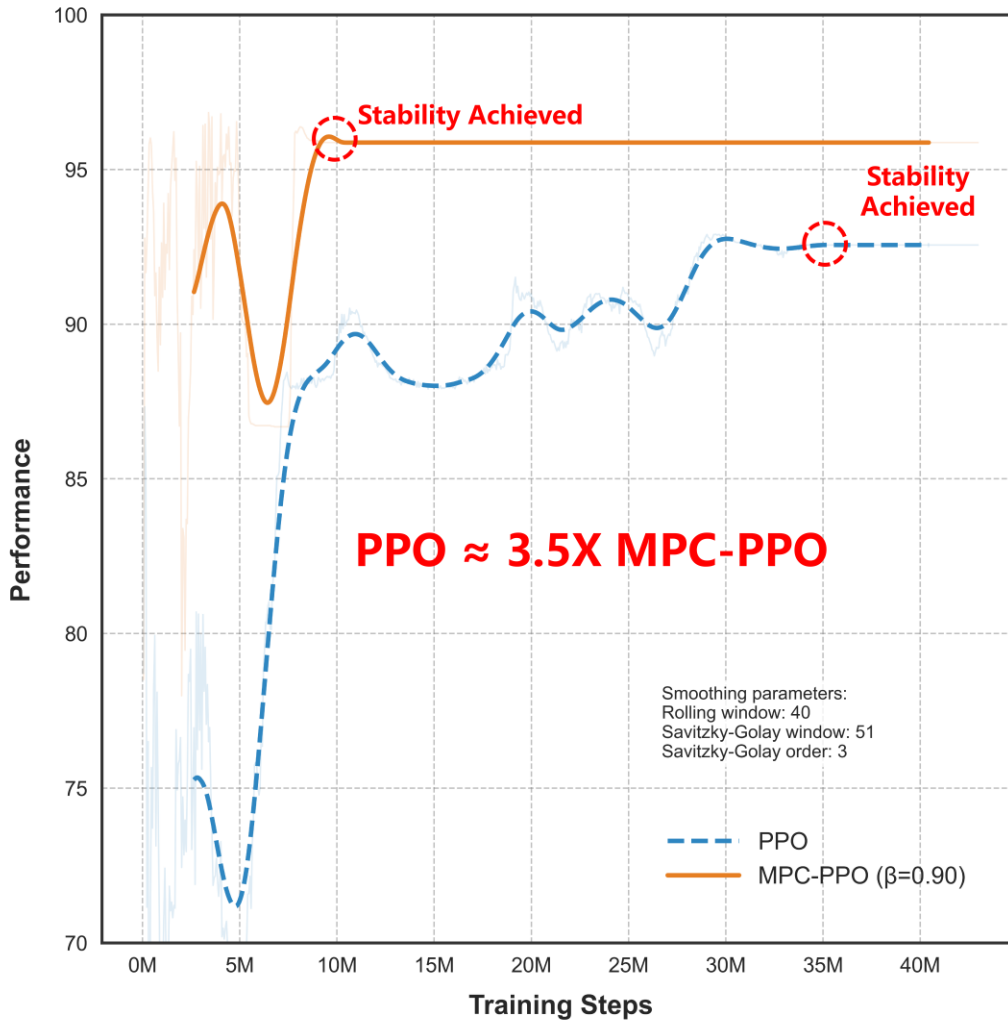


**Fig. 8. Performance metric comparison between traditional PPO and MPC-PPO during training process.**

MPC and MPC-PPO performed similarly in ventilation control rewards (99.36 vs 99.19). MPC, based on precise system models, achieved near-optimal ventilation control within short time windows. While MPC-PPO, though slightly sacrificing single-point accuracy, gains stronger environmental adaptability through the generalization capability of its policy networks. Similarly, Zhang and Zhao (2025) discussed such trade-off between accuracy and adaptability in stable transfer learning-based control.

### 4.3 Dynamic Embedding Mechanism Performance

Final rewards for the experience integration strategies ranged between 92.45 and 96.31, indicating the advantages of the dynamic embedding mechanism (Table 5). The dynamic embedding strategy (threshold 90) achieved the highest reward of  $94.99 \pm 6.66$  with an improvement of 5.46 points in temperature control compared to the baseline. While all dynamic embedding performed almost similarly the one with the threshold 90 configuration slightly resulted in maximum final reward. There were no major differences in action and temperature change smoothness. Dynamic embedding (threshold 80, 70, 60 and 50) and fixed ratio (50%) both achieved rewards of  $100.00 \pm 0.00$  in action smoothness, while all dynamic embedding strategies achieved good control in temperature control smoothness.

**Table 5. Comparison of different experience integration strategy test results.**

Strategy	temp_reward (70%)	action_reward (5%)	change_reward (5%)	ventilation_reward (20%)	Final reward
<b>Dynamic Embedding (Threshold 90)</b>	<b>94.99 ± 6.66</b>	<b>99.65 ± 0.81</b>	<b>100.00 ± 0.00</b>	<b>99.19 ± 0.54</b>	<b>96.31 ± 4.71</b>
Dynamic Embedding (Threshold 80)	94.67 ± 9.79	100.00 ± 0.00	100.00 ± 0.00	100.00 ± 0.00	96.27 ± 6.85
Dynamic Embedding (Threshold 70)	94.62 ± 7.78	100.00 ± 0.00	100.00 ± 0.00	100.00 ± 0.00	96.23 ± 5.45
Dynamic Embedding (Threshold 60)	94.02 ± 10.49	100.00 ± 0.00	100.00 ± 0.00	100.00 ± 0.00	95.82 ± 7.34
Dynamic Embedding (Threshold 50)	94.05 ± 9.61	100.00 ± 0.00	100.00 ± 0.00	100.00 ± 0.00	95.84 ± 6.73
Fixed Ratio (90%)	91.64 ± 8.86	99.65 ± 1.20	99.94 ± 0.14	99.95 ± 0.18	94.12 ± 6.20
Fixed Ratio (70%)	92.62 ± 7.73	99.65 ± 1.20	99.91 ± 0.16	99.95 ± 0.18	94.80 ± 5.41
Fixed Ratio (50%)	92.85 ± 12.80	100.00 ± 0.00	99.88 ± 0.17	100.00 ± 0.00	94.99 ± 8.96
Fixed Ratio (30%)	92.36 ± 13.08	99.31 ± 1.62	100.00 ± 0.00	99.90 ± 0.24	94.60 ± 9.15
No Experience Integration	89.53 ± 9.86	99.65 ± 0.81	99.88 ± 0.17	99.02 ± 0.51	92.45 ± 6.95

The superiority of the proposed dynamic embedding to fixed ratio strategy is theoretically based on its capability of avoiding the cumulative distribution shift effect (Wamahiu et al., 2025). This relates the fact that when the system encounters low-reward policies, the dynamic embedding mechanism achieves precise intervention rather than blind intervention through selective experience replacement. Compared to research in other fields, traditional methods such as behavioral cloning (Lee and Zhang, 2021) and demonstration learning (Zhang et al., 2024) typically adopt fixed ratio experience mixing strategies, easily falling into the dilemma between imitation learning and autonomous exploration.

Meanwhile, the non-linear performance changes observed in fixed ratio strategies as replacement ratios varied can be explained by exploration-exploitation trade-off theory (Moradi et al., 2024). Decreasing ratios (i.e., 90% to 30%) could result in the first-decreasing-then-increasing trend because excessively high replacement ratios (90%) converge policies too much toward MPC experiences. High ratios limit autonomous exploration space unlike low ratios (e.g., 30%) that cannot sufficiently utilize high-quality prior knowledge and thus can increase probability of ineffective exploration. This finding is similar to the theory of conservative updates in policy improvement proposed by Huang et al. (2024) while provides an operational approach.

#### 4.4 Combined Feature Influential Analysis

Figure 9 shows test results for each feature group (Table 6) on key performance indicators. Final performance rewards ranged from 91.71 to 96.31 with a clear positive correlation between feature richness and performance. Feature decrease from 10 to 3 declined temperature control rewards significantly (from 94.99 to 88.19) with increased variability (SD from ±6.66 to ±12.27). The most difference appeared between the baseline (G1) and minimal feature group (G5), i.e., 4.6-point dropped in final rewards. From G1 to G5, final reward variability progressively increased (from ±4.71 to ±8.58), indicating that rich feature inputs not only improved control accuracy but also enhanced system robustness.

G1 through G5 showed a step-wise declining trend in temperature control reward with a significant transition from G3 (91.64±7.21) to G4 (88.43±12.00) as well as an increased variability (SD increase by

4.79). This indicates that historical features ( $\bar{T}$  and  $\bar{\alpha}$ ) have a critical impact on temperature control accuracy. Action\_reward, change\_reward, and ventilation\_reward exhibited significantly less dependence on feature count than temperature control indicators. These indicators maintained high-levels ( $\geq 99.65$ ) even in the minimal feature group G5, indicating that basic control stability can be achieved through limited features.

**Table 6. Progressive feature group design for greenhouse environment control.**

Group	Feature set	Feature Count	Accessibility
G1: Baseline	$T_{air}, T_{soil}, T_{water}, T_{wall}, \alpha_{vent}, h, m, d, \bar{T}, \bar{\alpha}$	10	Low
G2: Extended	$T_{air}, \alpha_{vent}, h, m, d, \bar{T}, \bar{\alpha}$	7	Medium
G3: Enhanced	$T_{air}, \alpha_{vent}, h, \bar{T}, \bar{\alpha}$	5	Medium
G4: Basic	$T_{air}, \alpha_{vent}, h, m, d$	5	High
G5: Minimal	$T_{air}, \alpha_{vent}, h$	3	High

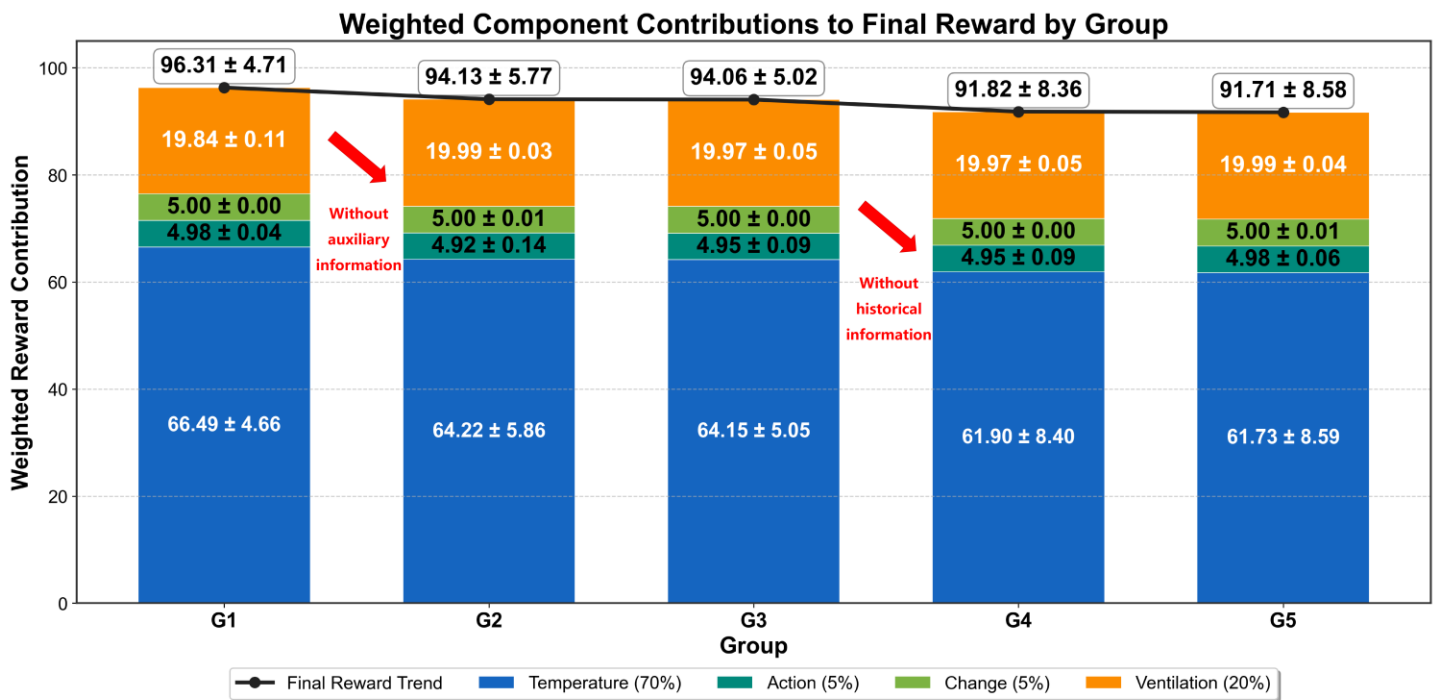


**Fig. 9. Control effect and weighted component contributions to final reward by group.**

Figure 10 shows the influence of various parameters on performance indicators. The historical window opening parameter had the most significant impact on overall system performance, with the highest absolute SHAP value contribution (7.449). This was successively followed by air temperature (4.905), historical temperature (4.747), wall temperature (0.190) and soil temperature (0.137). These results along with the cliff-like performance drop from G3 to G4 confirmed the critical role of historical information in greenhouse climate control.

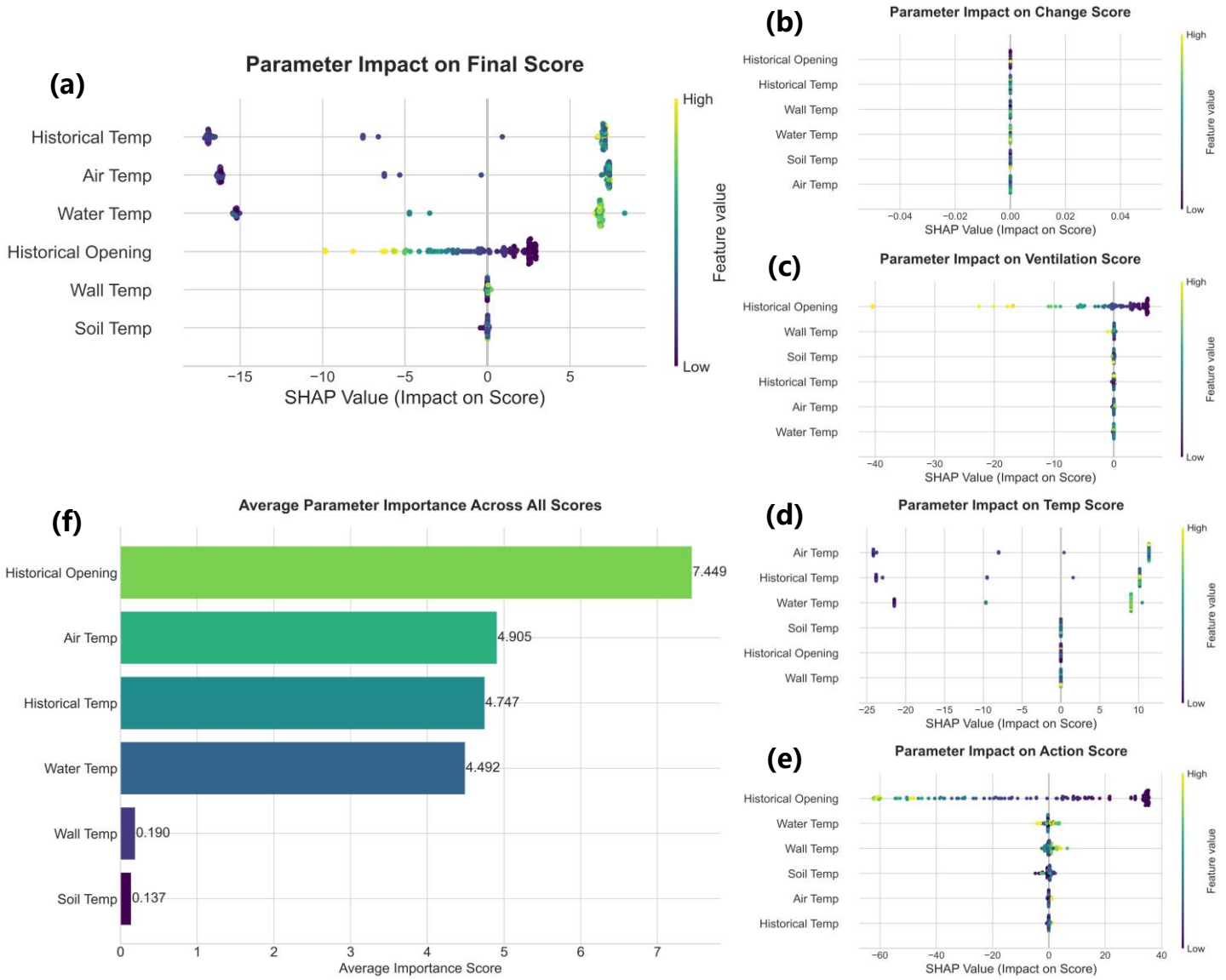


**Fig. 10. Environmental parameter influence mechanism analysis based on SHAP values. (a) Parameter impact on final comprehensive reward; (b) Parameter impact on temperature change stability reward; (c) Parameter impact on ventilation control reward; (d) Parameter impact on temperature control reward; (e) Parameter impact on execution action smoothness reward; (f) Average importance ranking of parameters across all performance indicators.**

The positive correlation between feature richness and performance confirms that decision quality is limited by information completeness (Iddio et al., 2020). The significant performance decline from G3 to G4 corresponds to removing historical features ( $\bar{T}$  and  $\bar{\alpha}$ ), and hence, presenting greenhouse environments as non-Markovian processes with strong memory effects. These historical features provide implicit memory, enabling the system to capture periodic patterns and long-term trends. In turn, systems achieve precise temperature prediction and control similar to the report by Lindemann et al. (2021) on historical embedding representations in time series prediction.

Rich feature inputs can construct multi-dimensional information spaces that enhance environmental state representation (Lindemann et al., 2021). Physical features, i.e., soil temperature and wall temperature, provide internal state information of the greenhouse thermodynamic system. This serves as information amplifiers that enhance future state prediction accuracy through indirect but critical indicators.

Notably, low-weight action\_reward and change\_reward showed minimal sensitivity to feature count because the stability indicators primarily depend on intrinsic control strategy rather than environmental state representation. The G2 group should be practically feasible as this differed by only 2.18 points from G1 while significantly reducing sensor deployment complexity – a finding from Goldenits et al. (2024) who emphasized on balancing performance and complexity in resource-constrained agricultural environments.

### 4.5 Model Generalization Performance Evaluation

Figure 11 details the performance results of PPO, MPC, and PID control methods across Shandong, Hebei, and Beijing regions. Final rewards (80.62 to 99.12) for the methods across regions showed clear regional correlation and methodological differentiation. All control methods performed best in Beijing (95.98 to 99.12), followed by Hebei (90.23 to 95.44), and the lowest in Shandong (80.62 to 85.80). The regional performance differences reflect the significant influence of climate conditions on control effectiveness.

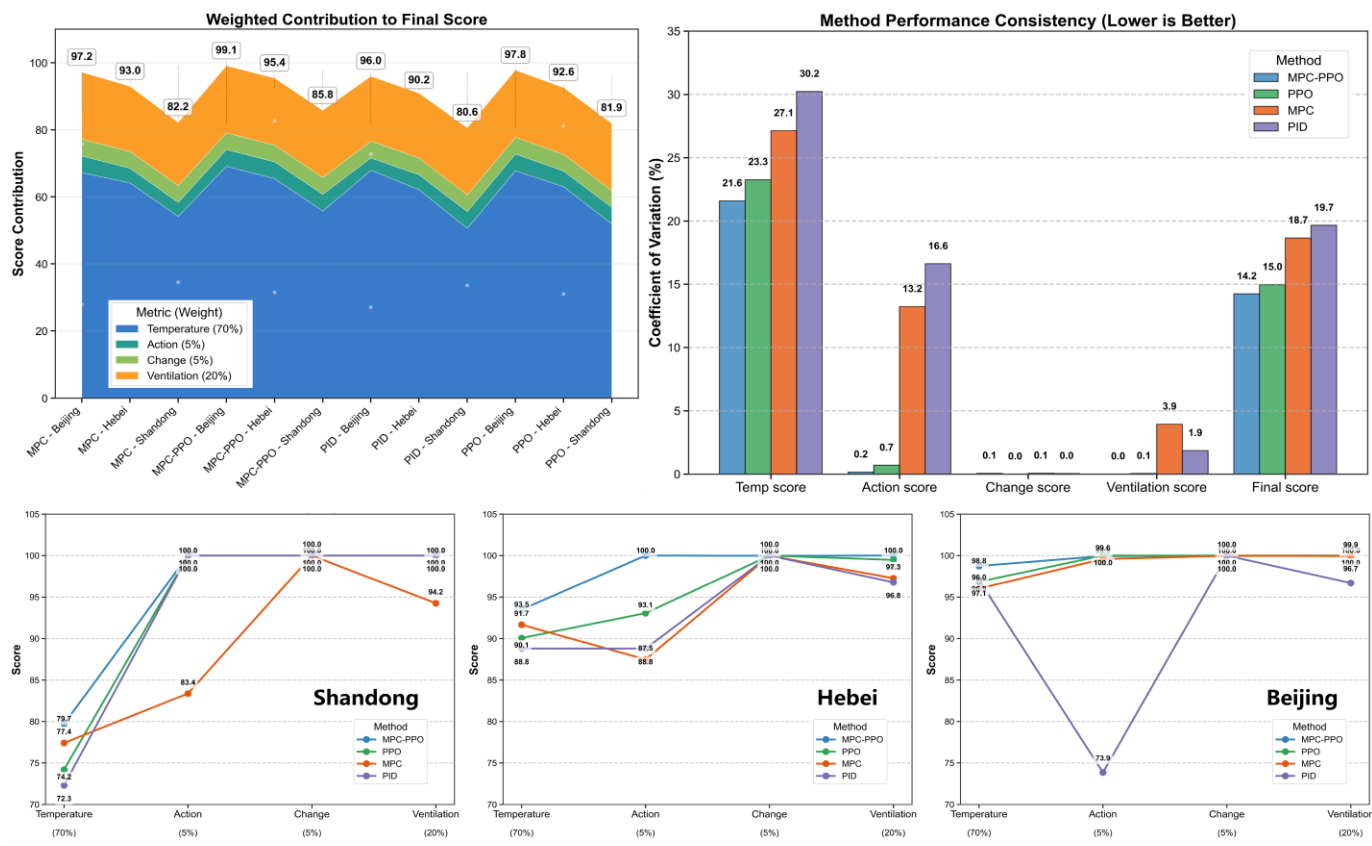


Fig. 11. Cross-regional model generalization performance comparison.

The MPC-PPO coupled framework achieved optimal performance in all test regions. MPC-PPO still maintained an effective control rate of 85.80% in Shandong region with an advancing MPC method by 3.59 points. MPC-PPO in Beijing achieved near-perfect control effectiveness of  $99.12 \pm 3.07$ . Temperature control indicators (70% weight) showed the highest regional variation. In Shandong, temperature control rewards were relatively low (72.31 to 79.71) with large fluctuations in all methods. The same control methods achieved high-accuracy control (96.03 to 98.75) with significantly reduced fluctuations in Beijing. MPC-PPO demonstrated excellent performance in action smoothness and ventilation controls ( $100.00 \pm 0.00$ ). Meanwhile, PID controllers were most unstable in action smoothness, particularly in Beijing (reward = 73.86).

The performance variations correspond to regional climate differences identified in Table 1. Controlling Shandong's greenhouse environment is known for complexity as this had the lowest average

temperature (13.24°C) and highest temperature variation (CV=40.28%). Similarly, Iddio et al. (2020) concluded that increased environmental uncertainty significantly increases greenhouse control complexity. In such a complex context, MPC-PPO achieved effective response to high-entropy environments by combining deterministic model prediction with probabilistic policy optimization, a mechanism theoretically consistent with the energy-efficient robust RL framework proposed by Ajagekar et al. (2023).

Good results for Beijing climate stemmed from its moderate climate, i.e., the lowest air temperature variation (24.59%) and stable wall temperatures (CV=9.30%) that provided constant boundary conditions and reduced control difficulty. This aligns with Zhang et al. (2016), who reported the impact of boundary conditions on system controllability when studying greenhouse thermodynamic models. The poor stability of PID can be attributed to PID controllers' inherent limitation in handling the region's larger daily temperature fluctuations (Zhao et al., 2019), which triggers frequent compensatory adjustments that exceed stability thresholds.

MPC-PPO's advantages were most pronounced in complex environments due to complementary learning paradigms when facing environmental parameter distribution shifts. Through dynamic experience embedding, it enables policy networks to quickly anchor near MPC-provided sub-optimal solutions before achieving local optimization. This is how MPC-PPO effectively addressed generalization challenges from distribution shifts while solved cold start problems more effectively than the framework proposed by Ajagekar et al. (2023).

## 4.6 Limitations and Future Way Forward

Despite the advantages of MPC-PPO framework in greenhouse environment control, several limitations are identified that need further investigation in the future study. For example:

(1) Current models focused mainly on temperature as the first attempt while ignoring comprehensive control of humidity, light and CO<sub>2</sub> concentration. Future research should, therefore, focus on developing multi-parameters coupled control systems.

(2) This study covered only winter growing seasons across three northern Chinese provinces, however, despite having high importance the spatiotemporal representation is quite compromised. This study recommends future work to expand data collection to diverse geographical regions and climate conditions.

(3) The proposed model required higher computational resources than PID algorithms and insufficiently addressed crop variety and growth stages. In turn, a future development should focus on lightweight algorithm implementation with customized strategies for different crop characteristics. Integration of environmental control with crop growth models to create comprehensive solutions from control to yield prediction would be an interesting topic to explore.

## 5. Conclusion

We proposed a teacher-student MPC-PPO coupled control framework for winter temperature control in northern China's solar greenhouses. It employed deep integration of MPC with policy optimization algorithms. The research designed a layered modeling strategy, multi-objective reward function, and reward-based adaptive experience replacement strategy, validated in solar greenhouses across three northern Chinese provinces. Key conclusions are:

(1) The MPC-PPO coupled framework is effective to control greenhouse environment. The MPC-PPO method outperformed traditional MPC system in temperature control ( $94.99 \pm 6.66$  vs  $92.19 \pm 12.80$ ) by 2.8

points. Besides, MPC-PPO reduced standard deviation in controlled temperature by nearly half. The MPC-PPO method ( $96.31 \pm 4.71$ ) significantly outperformed PID, PPO, MPC control methods with improved stability.

(2) The dynamic embedding strategy (threshold 90) improved temperature control rewards by 5.46 points compared to the non-experience integration baseline and reduced control fluctuations. Compared to fixed ratio strategies, the dynamic embedding mechanism solved policy distribution shift problems through selective experience replacement, balancing between knowledge utilization and autonomous exploration.

(3) Input feature richness positively correlated with system control performance. As feature count decreased from 10 to 3, temperature control rewards declined from 94.99 to 88.19 with increased variability (standard deviation =  $\pm 6.66$  to  $\pm 12.27$ ). Historical average temperature and average window opening impacted temperature control accuracy - their removal can decline performance by 3.21 points.

(4) The MPC-PPO framework demonstrated excellent cross-regional generalization capability and environmental adaptability. MPC-PPO maintained efficient control even with significant environmental distribution shifts: achieving near-perfect control effectiveness in Beijing (reward of  $99.12 \pm 3.07$ ), maintaining stable performance in Hebei (reward of  $95.44 \pm 4.85$ ) and maintaining a control rate of  $85.80 \pm 7.42$  in the most challenging Shandong region.

The main contribution of this study lies in constructing an intelligent ventilation control system for solar greenhouses with efficient training, multi-objective coordination, and cross-environmental adaptation capabilities. MPC-PPO method through deep integration of MPC and policy optimization algorithms solves problems of insufficient MPC model demand response and low PPO sampling efficiency. The proposed framework not only achieves multi-objective balance among temperature control accuracy, system stability, and energy efficiency, but also demonstrates good environmental adaptability and cross-regional generalization capabilities.

### **Declaration of competing interest**

The authors declare that they have no known competing financial interests or personal relationships that could have appeared to influence the work reported in this paper.

### **Acknowledgments**

Thanks to the support from Shandong Key Research and Development Program, China (04z0001108), the Open Fund of Key Laboratory of Smart Agriculture Technology in Yangtze River Delta, Ministry of Agriculture and Rural Affairs, China (KSAT-YRD2023002), the Youth Fund of Beijing Academy of Agriculture and Forestry Sciences, China (QNJJ202410), and the Reform and Development Project of Beijing Academy of Agriculture and Forestry Sciences, China.

### **Data availability**

The data that has been used is confidential.

## **References**

Abir Ahsan, T.M., Rahman, Md.S., Ahamed, Md.S., 2025. Geothermal energy application for greenhouse microclimate management: A review. *Geothermics* 127, 103209. <https://doi.org/10.1016/j.geothermics.2024.103209>

- Adesanya, M.A., Obasekore, H., Rabiou, A., Na, W.-H., Ogunlowo, Q.O., Akpenpuun, T.D., Kim, M.-H., Kim, H.-T., Kang, B.-Y., Lee, H.-W., 2024. Deep reinforcement learning for PID parameter tuning in greenhouse HVAC system energy Optimization: A TRNSYS-Python cosimulation approach. *Expert Systems with Applications* 252, 124126. <https://doi.org/10.1016/j.eswa.2024.124126>
- Ajagekar, A., Mattson, N.S., You, F., 2023. Energy-efficient AI-based control of semi-closed greenhouses leveraging robust optimization in deep reinforcement learning. *Adv. Appl. Energy* 9, 100119. <https://doi.org/10.1016/j.adapen.2022.100119>
- Arshad, A., Cîmpeanu, S.M., Jerca, I.O., Sovorn, C., Ali, B., Badulescu, L.A., Drăghici, E.M., 2024. Assessing the growth, yield, and biochemical composition of greenhouse cherry tomatoes with special emphasis on the progressive growth report. *BMC Plant Biol* 24, 1002. <https://doi.org/10.1186/s12870-024-05701-5>
- Bi, X., Ma, Q., Wang, X., Zhang, X., 2024. Application of phase change material on solar-greenhouse back wall and its effects on indoor thermal environment and cucumber production in winter. *Journal of Building Engineering* 93, 109883. <https://doi.org/10.1016/j.jobbe.2024.109883>
- Chen, D., Huang, Y., 2025. Integrating reinforcement learning and large language models for crop production process management optimization and control through a new knowledge-based deep learning paradigm. *Comput. Electron. Agric.* 232, 110028. <https://doi.org/10.1016/j.compag.2025.110028>
- Ding, Y., Wang, L., Li, Y., Li, D., 2018. Model predictive control and its application in agriculture: a review. *Comput. Electron. Agric.* 151, 104–117. <https://doi.org/10.1016/j.compag.2018.06.004>
- El Ghoumari, M.Y., Tantau, H.-J., Serrano, J., 2005. Non-linear constrained MPC: real-time implementation of greenhouse air temperature control. *Comput. Electron. Agric., Modelling and control in agricultural processes* 49, 345–356. <https://doi.org/10.1016/j.compag.2005.08.005>
- Fan, Z., Liu, Z., Li, Y., Zhang, J., Tu, G., Ding, T., 2024. New insights to boost the application potential of Chinese solar greenhouses in cold desert regions: System design and implementation. *Energy* 313, 133921. <https://doi.org/10.1016/j.energy.2024.133921>
- García-Mañas, F., Hägglund, T., Guzmán, J.L., Rodríguez, F., Berenguel, M., 2024. A practical solution for multivariable control of temperature and humidity in greenhouses. *European Journal of Control* 77, 100967. <https://doi.org/10.1016/j.ejcon.2024.100967>
- Gautron, R., Maillard, O.-A., Preux, P., Corbeels, M., Sabbadin, R., 2022. Reinforcement learning for crop management support: review, prospects and challenges. *Comput. Electron. Agric.* 200, 107182. <https://doi.org/10.1016/j.compag.2022.107182>
- Goldenits, G., Mallinger, K., Raubitzek, S., Neubauer, T., 2024. Current applications and potential future directions of reinforcement learning-based digital twins in agriculture. *Smart Agric. Technol.* 8, 100512. <https://doi.org/10.1016/j.atech.2024.100512>
- He, M., Wan, X., Liu, H., Xia, T., Gong, Z., Li, Y., Liu, X., Li, T., 2025. Theory and application of sustainable energy-efficient solar greenhouse in China. *Energy Conversion and Management* 325, 119394. <https://doi.org/10.1016/j.enconman.2024.119394>
- Huang, L., Dong, B., Zhang, W., 2024. Efficient offline reinforcement learning with relaxed conservatism. *IEEE Trans. Pattern Anal. Mach. Intell.* 46, 5260–5272. <https://doi.org/10.1109/TPAMI.2024.3364844>
- Iddio, E., Wang, L., Thomas, Y., McMorrow, G., Denzer, A., 2020. Energy efficient operation and modeling for greenhouses: a literature review. *Renewable Sustainable Energy Rev.* 117, 109480. <https://doi.org/10.1016/j.rser.2019.109480>

- Kim, Y.-S., Kim, M.K., Fu, N., Liu, J., Wang, J., Srebric, J., 2025. Investigating the impact of data normalization methods on predicting electricity consumption in a building using different artificial neural network models. *Sustainable Cities Soc.* 118, 105570. <https://doi.org/10.1016/j.scs.2024.105570>
- Kumar, A., Patel, V.K., 2023. Classification and identification of disease in potato leaf using hierarchical based deep learning convolutional neural network. *Multimedia Tools Appl.* 82, 31101–31127. <https://doi.org/10.1007/s11042-023-14663-z>
- Kyriakidis, L., Mendez, M.A., Bähr, M., 2024. A hybrid algorithm based on bayesian optimization and interior point OPTimizer for optimal operation of energy conversion systems. *Energy* 312, 133416. <https://doi.org/10.1016/j.energy.2024.133416>
- Ladosz, P., Weng, L., Kim, M., Oh, H., 2022. Exploration in deep reinforcement learning: a survey. *Inf. Fusion* 85, 1–22. <https://doi.org/10.1016/j.inffus.2022.03.003>
- Lee, Z.E., Zhang, K.M., 2021. Generalized reinforcement learning for building control using behavioral cloning. *Appl. Energy* 304, 117602. <https://doi.org/10.1016/j.apenergy.2021.117602>
- Li, H., He, H., 2024. Multiagent trust region policy optimization. *IEEE Trans. Neural Netw. Learn. Syst.* 35, 12873–12887. <https://doi.org/10.1109/TNNLS.2023.3265358>
- Li, Y., Sun, D., Xia, T., Varbanov, P.S., Liu, X., Li, T., 2023. Performance of a novel internal insulation in Chinese solar greenhouse for the cleaner and energy-saving production in high latitudes and cold regions. *Journal of Cleaner Production* 412, 137442. <https://doi.org/10.1016/j.jclepro.2023.137442>
- Lindemann, B., Müller, T., Vietz, H., Jazdi, N., Weyrich, M., 2021. A survey on long short-term memory networks for time series prediction. *Procedia CIRP*, 14th CIRP Conference on Intelligent Computation in Manufacturing Engineering, 15-17 July 2020 99, 650–655. <https://doi.org/10.1016/j.procir.2021.03.088>
- Liu, X., Zhu, T., Jiang, C., Ye, D., Zhao, F., 2022. Prioritized experience replay based on multi-armed bandit. *Expert Syst. Appl.* 189, 116023. <https://doi.org/10.1016/j.eswa.2021.116023>
- Mahmood, F., Govindan, R., Bermak, A., Yang, D., Al-Ansari, T., 2023. Data-driven robust model predictive control for greenhouse temperature control and energy utilisation assessment. *Appl. Energy* 343, 121190. <https://doi.org/10.1016/j.apenergy.2023.121190>
- Mallick, S., Airaldi, F., Dabiri, A., Sun, C., De Schutter, B., 2025. Reinforcement learning-based model predictive control for greenhouse climate control. *Smart Agricultural Technology* 10, 100751. <https://doi.org/10.1016/j.atech.2024.100751>
- Moradi, M., Zhai, Z.-M., Panahi, S., Lai, Y.-C., 2024. Adaptive network approach to exploration–exploitation trade-off in reinforcement learning. *Chaos: Interdiscip. J. Nonlinear Sci.* 34, 123120. <https://doi.org/10.1063/5.0221833>
- Morato, M.M., Felix, M.S., 2024. Data Science and Model Predictive Control: A survey of recent advances on data-driven MPC algorithms. *Journal of Process Control* 144, 103327. <https://doi.org/10.1016/j.jprocont.2024.103327>
- Morcego, B., Yin, W., Boersma, S., Van Henten, E., Puig, V., Sun, C., 2023. Reinforcement Learning versus Model Predictive Control on greenhouse climate control. *Computers and Electronics in Agriculture* 215, 108372. <https://doi.org/10.1016/j.compag.2023.108372>
- Peng, Y., Zeng, J., Hu, Y., Fang, Q., Yin, Q., 2024. Reinforcement learning from suboptimal demonstrations based on reward relabeling. *Expert Syst. Appl.* 255, 124580. <https://doi.org/10.1016/j.eswa.2024.124580>

- Platero-Horcajadas, M., Pardo-Pina, S., Cámara-Zapata, J.-M., Brenes-Carranza, J.-A., Ferrández-Pastor, F.-J., 2024. Enhancing Greenhouse Efficiency: Integrating IoT and Reinforcement Learning for Optimized Climate Control. *Sensors* 24, 8109. <https://doi.org/10.3390/s24248109>
- Qi, D., Zhang, K., Zhao, C., Li, Ang, Song, B., Li, Angui, 2024. Optimized model predictive control for solar assisted earth air heat exchanger system in greenhouse. *Renewable Energy* 228, 120582. <https://doi.org/10.1016/j.renene.2024.120582>
- Rio, A.D., Jimenez, D., Serrano, J., 2024. Comparative Analysis of A3C and PPO Algorithms in Reinforcement Learning: A Survey on General Environments. *IEEE Access* 12, 146795–146806. <https://doi.org/10.1109/ACCESS.2024.3472473>
- Shi, Y., An, L., Guo, S., Li, J., Sun, H., Zhang, R., Zhao, H., Bai, L., Hou, L., Zhang, Y., Ahammed, G.J., 2025. Nano silicon causes a shift in rhizospheric soil microbial community structure and improves nutrient uptake and assimilation in tomato plants under low temperature. *Soil and Tillage Research* 248, 106451. <https://doi.org/10.1016/j.still.2025.106451>
- Svensen, J.L., Cheng, X., Boersma, S., Sun, C., 2024. Chance-constrained stochastic MPC of greenhouse production systems with parametric uncertainty. *Comput. Electron. Agric.* 217, 108578. <https://doi.org/10.1016/j.compag.2023.108578>
- Wamahiu, K., Kala, J., Evans, J., 2025. Assessing the influence of bias correction of boundary conditions, spectral nudging and model parameterisation on model errors and climate change signals for regional climate model simulations. *Clim. Dyn.* 63, 138. <https://doi.org/10.1007/s00382-025-07634-7>
- Wang, B., Sun, Z., Jiang, X., Zeng, J., Liu, R., 2023. Kalman filter and its application in data assimilation. *Atmosphere* 14, 1319. <https://doi.org/10.3390/atmos14081319>
- Wang, L., He, X., Luo, D., 2020. Deep reinforcement learning for greenhouse climate control, in: 2020 IEEE International Conference on Knowledge Graph (ICKG). Presented at the 2020 IEEE International Conference on Knowledge Graph (ICKG), pp. 474–480. <https://doi.org/10.1109/ICKG50248.2020.00073>
- Wang, Y., Wang, P., Tansey, K., Liu, J., Delaney, B., Quan, W., 2025. An interpretable approach combining shapley additive explanations and LightGBM based on data augmentation for improving wheat yield estimates. *Comput. Electron. Agric.* 229, 109758. <https://doi.org/10.1016/j.compag.2024.109758>
- Xu, X.-Y., Chen, Y.-Y., Liu, T.-R., 2024. TD3-BC-PPO: Twin delayed DDPG-based and behavior cloning-enhanced proximal policy optimization for dynamic optimization affine formation. *Journal of the Franklin Institute* 361, 107018. <https://doi.org/10.1016/j.jfranklin.2024.107018>
- Xu, Y., Zhang, H., 2024. Convergence of deep ReLU networks. *Neurocomputing* 571, 127174. <https://doi.org/10.1016/j.neucom.2023.127174>
- Yang, L., Ding, J., Ge, H., 2024. Structure modification based PID neural network decoupling control for nonlinear multivariable systems. *Inf. Sci.* 681, 121222. <https://doi.org/10.1016/j.ins.2024.121222>
- Yu, J., Zhao, J., Sun, C., Zhang, R., Zheng, W., Xu, L., Wei, X., 2025. A dual deep learning approach for winter temperature prediction in solar greenhouses in Northern China. *Computers and Electronics in Agriculture* 229, 109807. <https://doi.org/10.1016/j.compag.2024.109807>
- Yu, J., Zheng, W., Xu, L., Zhangzhong, L., Zhang, G., Shan, F., 2020. A PSO-XGBoost Model for Estimating Daily Reference Evapotranspiration in the Solar Greenhouse. *Intell Autom Soft Co*, 无 26, 989–1003. <https://doi.org/10.32604/iasc.2020.010130>

- Zhang, B., Li, G., Zhang, J., Bai, X., 2024. A reliable traversability learning method based on human-demonstrated risk cost mapping for mobile robots over uneven terrain. *Eng. Appl. Artif. Intell.* 138, 109339. <https://doi.org/10.1016/j.engappai.2024.109339>
- Zhang, H., Zhao, C., 2025. Stable transfer learning-based control: an off-dynamics adaptive approach for unknown nonlinear systems. *Neurocomputing* 616, 128951. <https://doi.org/10.1016/j.neucom.2024.128951>
- Zhang, X., Wang, H., Zou, Z., Wang, S., 2016. CFD and weighted entropy based simulation and optimisation of chinese solar greenhouse temperature distribution. *Biosyst. Eng.* 142, 12–26. <https://doi.org/10.1016/j.biosystemseng.2015.11.006>
- Zhao, B.Y., Zhao, Z.G., Li, Y., Wang, R.Z., Taylor, R.A., 2019. An adaptive PID control method to improve the power tracking performance of solar photovoltaic air-conditioning systems. *Renew. Sustain. Energy Rev.* 113, 109250. <https://doi.org/10.1016/j.rser.2019.109250>
- Zhou, P., Xie, X., Lin, Z., Yan, S., 2024. Towards understanding convergence and generalization of AdamW. *IEEE Trans. Pattern Anal. Mach. Intell.* 46, 6486–6493. <https://doi.org/10.1109/TPAMI.2024.3382294>
- Zhu, W., Rosendo, A., 2021. A functional clipping approach for policy optimization algorithms. *IEEE Access* 9, 96056–96063. <https://doi.org/10.1109/ACCESS.2021.3094566>